Fisher, A., Davis, E.E., and Escutia, C. (Eds.), 2000
Proceedings of the Ocean Drilling Program, Scientific Results, Vol. 168

12. MAJOR AND TRACE ELEMENT COMPOSITIONS OF SECONDARY CLAYS IN BASALTS ALTERED AT LOW TEMPERATURE, EASTERN FLANK OF THE JUAN DE FUCA RIDGE[1]

Sean Porter,[2] David A. Vanko,[2,3] and A. Mohamad Ghazi[2]

ABSTRACT

A drilling transect across the sedimented eastern flank of the Juan de Fuca Ridge, conducted during Leg 168 of the Ocean Drilling Program, resulted in the recovery of samples of volcanic basement rocks (pillow basalts, massive basalts, and volcanic glass breccias) that exhibit the effects of low-temperature hydrothermal alteration. Secondary clays are ubiquitous, with Mg-rich and Fe-rich saponite and celadonitic clays commonly accounting for several percent, and up to 10%–20% by volume. Present-day temperatures of the basement sites vary from 15° to 64°C, with the coolest site being about 0.8 Ma, and the warmest site being about 3.5 Ma. Whereas clays are abundant at sites that have been heated to present temperatures of 23°C and higher, the youngest site at 15°C has only a small trace of secondary clay alteration. Alteration increases as temperatures increase and as the volcanic basement ages.

The chemical compositions of secondary clays were determined by electron microprobe, and additional trace element data were determined by both conventional nebulization inductively coupled plasma-mass spectroscopy (ICP-MS) and laser-ablation ICP-MS. Trioctahedral saponite and pyrite are characteristic of the interior of altered rock pieces, forming under conditions of low-oxygen fugacity. Dioctahedral celadonite-like clays along with iron oxyhydroxide and Mg-saponite are characteristic of oxidized haloes surrounding the nonoxidized rock interiors. Chemical compositions of the clays are very similar to those determined from other deep-sea basalts altered at low temperature. The variable Mg:Fe of saponite appears to be a systematic function both of the Mg:Fe of the host rock and the oxidation state during water–rock interaction.

INTRODUCTION

A large flux of both heat and seawater occurs through hydrothermal circulation in the igneous crust of midocean ridge flanks, playing an important role in the alteration of the crust (Sclater et al., 1976; Anderson et al., 1977; Alt et al., 1986; Purdy, 1987; Davis et al., 1992; Mottl and Wheat, 1994; Stein and Stein, 19

94). Chemical fluxes from low-temperature alteration of midocean ridge basalts (MORBs) could be important in crust as old as 10 Ma, or as long as significant ridge-flank fluid flow occurs (Hart and Staudigel, 1986; Mottl and Wheat, 1994). Ocean Drilling Program Leg 168 was dedicated to studying ridge-flank hydrothermal processes near the Juan de Fuca Ridge (Davis, Fisher, Firth, et al., 1997).

Off-axis hydrothermal circulation can be broadly divided into "open" and "restricted" systems, where the former are colder and seawater dominated, and the latter are warmer and involve more altered basement fluids (Teagle et al., 1996). Alteration of the shallow crust is dominated initially by low-temperature and high oxygen-fugacity conditions during a ≤1-m.y. period of open seawater circulation. This may be followed by up to 10 m.y. of alteration resulting from more closed hydrothermal circulation at warmer temperatures (yet still ≤100°C) and low oxygen fugacity. The mineralogical record of oxidizing alteration includes Mg-rich saponite and K-bearing, Fe^{3+}-bearing celadonitic clays combined with complex iron oxyhydroxide ($Fe[O,OH]_x$) and clay mixtures (iddingsite). The mineralogic record of alteration under reducing conditions includes saponite and pyrite.

Basalts cored during Leg 168 on the eastern flank of the Juan de Fuca Ridge (JdFR) exhibit a variety of low-temperature alteration features, particularly clay minerals, $Fe(O,OH)_x$, and pyrite. Processes that formed saponite, celadonitic clay, and $Fe(O,OH)_x$ are superimposed in a variety of combinations (see Marescotti et al., Chap. 10, this volume). This paper reports on the chemical composition of a representative sampling of secondary clays produced during the low-temperature hydrothermal alteration of MORB recovered during Leg 168 and demonstrates that the major element and trace element chemistry of saponites and celadonitic clays vary within narrow limits.

ANALYTICAL METHODS

Sixty-five small specimens of volcanic rock were slabbed and fabricated into polished thin sections for standard petrographic analysis. Electron microprobe analyses were obtained from 23 representative thin sections using the JEOL 866 wavelength-dispersive instrument located at the University of Georgia in Athens, Georgia. Analyses were performed with 15-keV accelerating voltage, 5-na beam current, and 10-µm beam diameter and were calibrated using various well-characterized natural standards. Saponites were recalculated into a trioctahedral clay mineral formula by normalizing the electron microprobe analysis to 22 oxygens, then assigning eight Si + Al to the tetrahedral site, the remaining Al plus Ti, Fe^{2+}, Mn, and Mg to the six octahedral cation sites, and any excess Mg, Ca, and Na to the interlayer cation site. Celadonite formulas were recalculated by normalizing the electron microprobe analysis so that the sum of tetrahedral plus octahedral cations is twelve, and then partitioning Fe into ferrous and ferric iron in such a way as to achieve a total negative charge of 44 per formula unit. The result is an electrostatically balanced dioctahedral mica formula (Li et al., 1997).

Five specimens that had enough clay mineral for manual separation were selected for reconnaissance determinations of a suite of minor and trace elements by inductively coupled plasma-mass spectroscopy (ICP-MS), using the Finnigan MAT Sola ICP-MS at Georgia State University, Atlanta, Georgia. These specimens were studied by X-ray diffractometry (with an automated Philips Norelco XRD using CuK_α radiation) to ensure purity of the clay mineral and to confirm its crystal structure. One sample was fashioned into a polished thick section for reconnaissance laser-ablation ICP-MS analysis. The laser used for microsample ablation operates at 266 nm in the UV region and was operated in the Q-switched mode at 4-Hz repetition and with 4 mJ per pulse. The laser was focused on the clay sample surface and

[1] Fisher, A., Davis, E.E., and Escutia, C. (Eds.), 2000. *Proc. ODP, Sci. Results,* 163: College Station TX (Ocean Drilling Program).
[2]Department of Geology, Georgia State University, Atlanta GA 30303, USA.
[3]Correspondence author: dvanko@gsu.edu

produced an ablation pit with a diameter of about 40 µm. An argon stream introduced the ablated material as a wet plasma into the ICP torch, and the quadrupole mass spectrometer was set to acquire data continuously during three scans (over about 20 s) using a secondary electron multiplier detector.

Quantification for LA–ICP-MS was accomplished using the National Institute of Standards and Technology standard reference material 611 (SRM-611), which contains numerous trace elements at about 500 ppm. The procedures followed closely those reported by Perkins and Pearce (1995), Kontak and Jackson (1995), and Jenner et al. (1993). Magnesium, present in SRM-611 at 500 ppm and in the clay mineral at about 17 wt% MgO, served as an internal standard to correct for differences in the ablation yields between the SRM-611 glass and the clay sample. Further analytical details are given in the Appendix of Yatabe et al. (Chap. 11, this volume).

RESULTS

Background

The Juan de Fuca Ridge (JdFR), which produces ocean crust at a half-rate of 29 mm/yr, is located a few hundred kilometers off the western coast of North America. The topographic relief of the ridge produces a barrier to terrigenous turbidite sediment supplied from Pleistocene glacial sources along the continental margin. This has resulted in the accumulation of an onlapping layer of sediment that buries the eastern flank of the JdFR within a few tens of kilometers of the ridge crest, where the crust at some locations is less than 1 Ma. This area provided several targets for studying ridge-flank hydrothermal processes during Leg 168 (Davis, Fisher, Firth, et al., 1997). Three distinct fluid-flow regimes were evaluated by drilling a transect normal to the JdFR (Fig. 1). These were (1) a transition zone between sediment-free (permitting open hydrothermal circulation) and sediment-covered (hydrologically sealed) igneous crust, named the Hydrothermal Transition (HT) area; (2) an area where rugged basement topography, large lateral variations in sediment thickness, and small, isolated basement outcrops are all inferred to influence the patterns and rates of fluid flow in and out of the basement, named the Rough Basement (RB) area; and (3) an area where a uniform and regionally continuous cover of sediments over less rugged basement topography largely prevents crust–ocean fluid exchange and impedes heat flow, named the Buried Basement (BB) transect. Ten drilling sites were designed to sample sediments, rocks, and fluid across these transects (Fig. 1).

Altered basalts investigated in this study come from the top of the volcanic basement in nine of these boreholes where the present-day temperatures determined during Leg 168 vary from 15° to 64°C (Davis, Fisher, Firth, et al., 1997). Progressive changes in alteration style are related to the increased age, closed-system nature, and alteration temperature of the samples (Davis, Fisher, Firth, et al., 1997; Marescotti et al., Chap. 10, this volume).

All of the igneous rocks recovered during Leg 168 exhibit secondary alteration affects, forming pervasively or as discrete fracture-parallel alteration haloes. Secondary minerals, most commonly clays, iron oxyhydroxides, and carbonates, are found lining or filling vesicles, coating fracture surfaces as veins, and replacing phenocrysts and groundmass. The total amount of alteration varies widely from about 1 to 24 volume percent secondary minerals. In general, the more easterly samples, which are also presently at higher temperatures, exhibit more alteration (see Marescotti et al., Chap. 10, this volume).

Petrography

Saponite is cryptocrystalline or fibrous. It is typically green to blue in hand specimen and pale brown to yellowish and olive green in thin section (Davis, Fisher, Firth, et al., 1997). Celadonite is the descriptive term used for the cryptocrystalline to fibrous, strongly green colored clay in thin sections. Saponite forms characteristically in the less altered interiors of rock pieces, usually associated only with secondary pyrite. Celadonite is more typically present in the oxidized haloes of rock pieces, associated with $Fe(O,OH)_x$. In the transitional zone between oxidizing and reducing areas, considerable overlap may result in sequential vesicle and vein fills. The observed sequences vary from saponite followed by celadonite to celadonite followed by saponite. Iddingsite (a clay-$Fe(O,OH)_x$ mixture) commonly fills

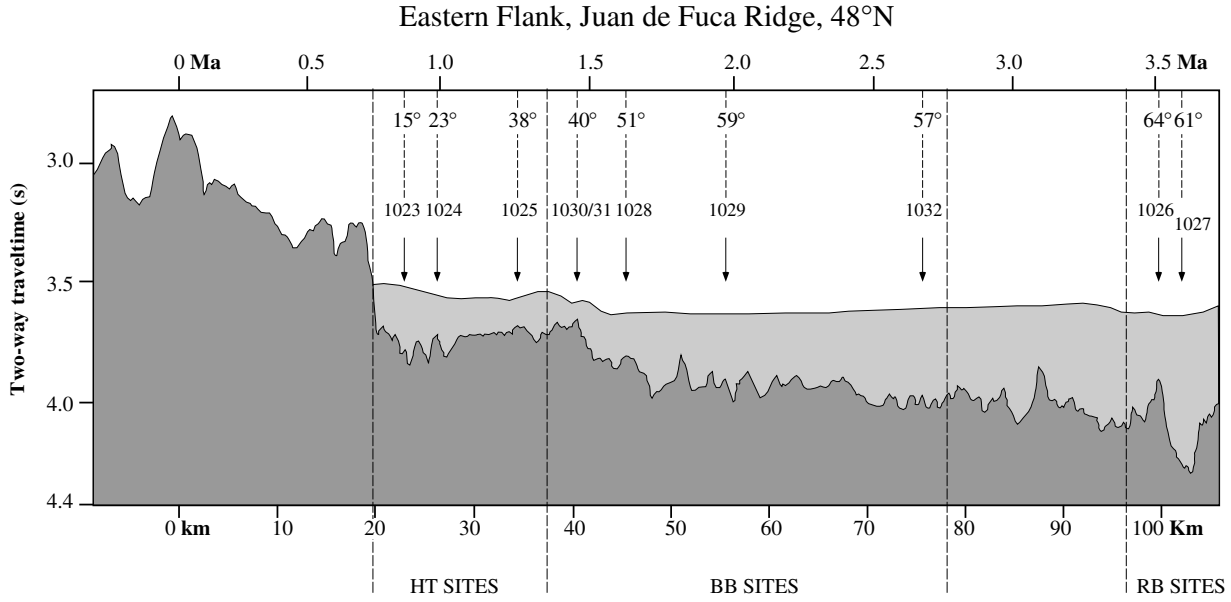

Figure 1. Basement topography (dark gray area) and sediment cover (light gray area), across the eastern flank of the Juan de Fuca Ridge at 48°N, derived from composite seismic reflection profiles, from Davis, Fisher, Firth, et al. (1997). The locations of the Leg 168 sites are shown, along with the estimated present-day temperature at the basement-sediment interface. HT = Hydrothermal Transition; BB = Buried Basement; RB = Rough Basement.

vesicles after celadonite. Photomicrographs of a variety of vesicles and veins showing the various filling sequences are shown in Davis, Fisher, Firth, et al. (1997) and discussed more fully in Marescotti et al. (Chap. 10, this volume).

Mineral Composition

X-ray diffraction results confirm that the darker green clays in veins and vesicles are trioctahedral varieties ($d_{(060)}$ = 1.528–1.540 Å) that expand upon glycolation and collapse on heating (Fig. 2). Electron microprobe analyses (Table 1; Fig. 3) confirm that they are saponite with very low interlayer potassium and variable Fe/(Fe + Mg). The formulas of bright green celadonitic clays (Table 2; Fig. 3) trend toward ideal celadonite, yet all exhibit a deficit of interlayer potassium. The formulas listed in Table 2 contain between 1.2 and 1.6 interlayer cations for eight tetrahedral cations, whereas the ideal celadonite formula requires two interlayer cations. This suggests either that a physical mixture with saponite or iron oxyhydroxide was actually analyzed, or that the material is really a poorly crystallized precursor to ideal celadonite (often referred to as protoceladonite [Adamson and Richards, 1990]). The compositions of saponite and celadonitic clays from Leg 168 are comparable to those of clays from many other altered seafloor basalts (e.g., Adamson and Richards, 1990; Alt, 1993; Desprairies et al., 1989; Gillis et al., 1992; Laverne et al., 1996; Teagle et al., 1996).

Trace elements were determined in a small number of samples that provided enough material for hand picking, digestion, and conventional nebulization in an ICP-MS (Table 3). In one specimen containing a 1-mm-thick saponite vein, a polished slab was prepared and studied by means of laser ablation ICP-MS (Table 4). Trace elements that were determined in saponite by both techniques exhibit good agreement. The strontium concentration, which was determined to be between 93 and 303 ppm with six different ablations, was determined by nebulization ICP-MS to vary from 0.4 to 140 ppm. Lanthanum and U concentrations were below the detection limits of around 16 ppm and 8 ppm by LA–ICP-MS, respectively, and they varied from 0.1 to 5.5 ppm La and 0.1 to 24 ppm U by nebulization ICP-MS. The cerium concentrations were below detection limits (<13 ppm) to 64 ppm by LA–ICP-MS, and 0.1–15 ppm by nebulization ICP-MS. The rubidium concentrations were below detection limits (<2 ppm) to 21 ppm by LA–ICP-MS, and around 9 ppm by nebulization ICP-MS. In all cases, the ranges determined for each element overlap.

Relative to an average MORB, the trace element patterns for the saponite show enrichment in a number of large-ion lithophile and high field-strength elements (Fig. 4A). However, normalized to the trace element concentrations in the host basalt (M. Constantin, pers. comm., 1998), the enrichment is not as strong (Fig. 4B). The saponite, in general, exhibits mild enrichment in Ba, Rb, Th, and U; depletion or no fractionation in Nb, the REE, and Sr; and either enrichment or depletion with respect to Zr and Hf.

DISCUSSION AND CONCLUSIONS

Secondary clays are ubiquitous alteration products in the Leg 168 volcanic rocks, varying in abundance from a trace to several percent, and varying mineralogically from celadonitic clays and Mg-saponite in oxidized alteration haloes to saponite only in the reduced alteration of rock interiors. All of the volcanic basement sites cored across the Leg 168 transect contain evidence of early oxidizing alteration, except for the few small rocks obtained at the westernmost HT site (Site 1023). This is because all of the sites initially were unsedimented areas of seafloor before they were buried by the sediments of the Cascadia Basin. Seawater-derived fluid that eventually gained access to the interiors of rock pieces, probably through slow diffusion, is inferred to have lost its potential for oxidation and instead affected these interiors in the form of a reducing alteration.

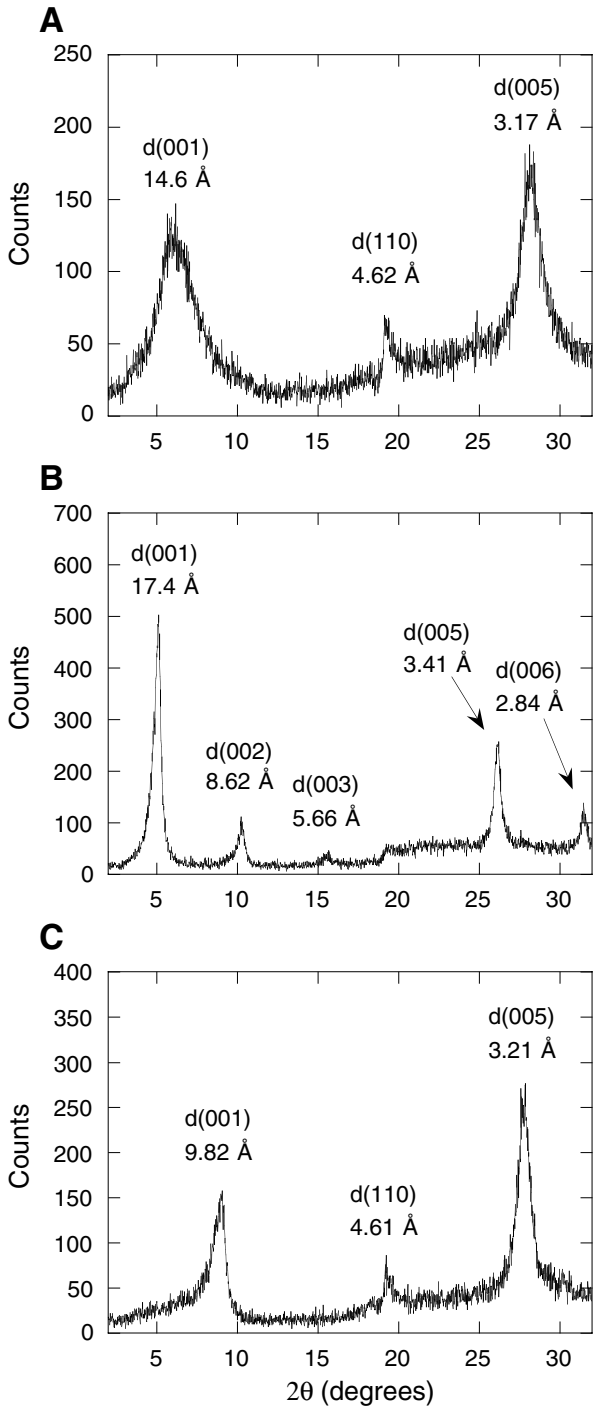

Figure 2. Representative X-ray diffraction patterns for a trioctahedral expandable saponite from Sample 168-1032A-13R-4, 21–29 cm (Piece 4). **A.** Clay sample, air dried. **B.** After glycolation for 24 hr. **C.** After heating at 400°C for 3 hr.

The Mg:Fe value in saponite may be controlled by the Mg:Fe value in coexisting solution and the oxygen fugacity of the solution. Marescotti et al. (Chap. 10, this volume) demonstrated that within individual specimens, saponite in oxidized haloes with celadonite is typically more Mg-rich than saponite in the reduced rock interiors. Superimposed on this effect, though, is a regional effect that can be recognized when saponite compositions from the whole Leg 168 transect are evaluated (Fig. 5). Pillow basalts from Leg 168 have an

Table 1. Representative electron microprobe saponite analyses.

Hole, core, section:	1027C-4R-1	1027C-4R-1	1027C-4R-1	1027C-1R-4	1032A-16R-1	1032A-16R-1	1032A-15R-2	1032A-15R-2	1032A-15R-2	1032A-15R-2	1032A-15R-2	1032A-15R-2	1032A-14R-1	1032A-14R-1	1023A-22X-CC	1025B-11X-CC	1025C-1R-2	1028A-15X-6
Piece:	18	18	15	1e	15	15	8	8	8	8	8	8	7	7	1	4	16	2
Interval (cm):	114-118	114-118	93-96	108-110	96-99	96-99	63-66	63-66	63-66	63-66	63-66	63-66	25-29	25-29	35-40	46-52	102-103	130-132
Occurrence:	Vesicle	Vesicle	Replacement	Replacement	Vesicle	Vesicle	Replacement	Replacement	Replacement	Replacement	Replacement	Replacement	Vesicle	Vesicle	Vesicle	Vesicle	Cavity filling	Vesicle
EMP Anl #:	5	6	24	37	44	45	46	47	48	49	53	56	61	62	73	85	92	111
SiO_2	45.49	45.61	46.18	44.68	46.25	46.55	52.42	53.72	53.18	49.37	42.05	44.39	48.44	46.63	43.26	38.94	48.98	50.71
TiO_2	0.01	0.02	0	0.37	0.07	0.15	0.05	0.04	0.04	0.04	0	0.02	0.02	0.07	0.27	0.08	0.06	0
Al_2O_3	4.91	4.51	4.64	5.80	3.36	4.35	1.73	1.47	1.89	2.45	4.40	5.33	3.84	3.25	4.84	4.56	2.38	2.89
FeO	12.84	13.32	15.16	17.56	7.73	11.54	10.13	9.86	9.25	7.62	13.48	12.83	10	8.87	12.21	17.32	16.85	12.78
MnO	0.07	0.05	0.03	0.19	0.10	0.06	0.12	0.28	0	0	0.06	0	0.07	0.09	0.03	0.18	0.25	0.07
MgO	17.42	17.59	15.95	16.92	19.97	18.58	21.58	22.54	23.09	21.94	17.12	17.13	20.46	19.66	15.55	11.44	15.99	19.36
CaO	1.03	1.09	0.85	1.39	0.69	0.85	0.68	0.43	0.49	0.39	0.73	1.35	0.76	0.72	0.69	1.06	0.74	0.46
Na_2O	0.82	0.73	0.85	0.55	0.65	0.93	0.70	0.37	0.71	0	0	0	0	0	0.51	0.44	0.46	0.59
K_2O	0.34	0.45	0.55	0.32	0.08	0.02	0.19	0.17	0.21	0.13	0.29	0.07	0.11	0.10	0.28	0.33	0.18	0.50
Cl	0.11	0.12	0.05	0.02	0.06	0	0.09	0.03	0.05	0.03	0.11	0.26	0.05	0.03	0.03	0.13	0.17	0.06
Ba	0.03	0	0.04															
Total	83.07	83.49	84.30	87.80	78.96	83.03	87.69	88.91	88.91	81.97	78.24	81.38	83.75	79.42	77.67	74.48	86.06	87.42
O = Cl	0.02	0.03	0.01	0.00	0.01	0.00	0.02	0.01	0.01	0.01	0.02	0.06	0.01	0.01	0.01	0.03	0.04	0.01
Total	83.05	83.46	84.29	87.80	78.95	83.03	87.67	88.90	88.90	81.96	78.22	81.32	83.74	79.41	77.66	74.45	86.02	87.41
# of oxygen	22	22	22	22	22	22	22	22	22	22	22	22	22	22	22	22	22	22
Tetrahedral Cations																		
Si(IV)	7.223	7.230	7.302	6.900	7.466	7.303	7.676	7.719	7.634	7.611	7.133	7.181	7.426	7.502	7.304	7.167	7.602	7.563
Al(IV)	0.777	0.770	0.698	1.056	0.534	0.697	0.299	0.249	0.320	0.389	0.867	0.819	0.574	0.498	0.696	0.833	0.398	0.437
Sum of (IV)	8.000	8.000	8.000	7.956	8.000	8.000	7.975	7.968	7.954	8.000	8.000	8.000	8.000	8.000	8.000	8.000	8.000	8.000
Octahedral																		
Al(VI)	0.143	0.073	0.168	0.000	0.106	0.108	0.000	0.000	0.000	0.057	0.014	0.199	0.121	0.119	0.267	0.157	0.038	0.071
Fe^{2+}	1.705	1.766	2.005	2.268	1.044	1.514	1.241	1.185	1.110	0.982	1.912	1.736	1.282	1.193	1.724	2.666	2.187	1.594
Mn	0.009	0.007	0.004	0.025	0.014	0.008	0.015	0.034	0.000	0.000	0.009	0.000	0.009	0.012	0.004	0.028	0.033	0.009
Ti	0.001	0.002	0.000	0.043	0.008	0.018	0.006	0.004	0.004	0.005	0.000	0.002	0.002	0.008	0.034	0.011	0.007	0.000
Mg	4.122	4.152	3.759	3.664	4.805	4.344	4.710	4.777	4.885	4.956	4.065	4.063	4.586	4.667	3.913	3.137	3.699	4.303
Sum of (VI)	5.981	6.000	5.936	6.000	5.976	5.991	5.970	6.000	6.000	6.000	6.000	6.000	6.000	6.000	5.943	6.000	5.963	5.977
Interlayer																		
Mg	0.000	0.004	0.000	0.230	0.000	0.000	0.000	0.050	0.055	0.085	0.263	0.067	0.089	0.047	0.000	0.001	0.000	0.000
Ca	0.175	0.185	0.144	0.230	0.119	0.143	0.107	0.066	0.075	0.064	0.133	0.234	0.125	0.124	0.125	0.209	0.123	0.074
Na	0.252	0.224	0.261	0.165	0.203	0.283	0.199	0.103	0.198	0.000	0.000	0.000	0.000	0.000	0.167	0.157	0.138	0.171
K	0.069	0.091	0.111	0.063	0.016	0.004	0.035	0.031	0.038	0.026	0.063	0.014	0.022	0.021	0.060	0.077	0.036	0.095
Sum interlayer	0.497	0.504	0.516	0.687	0.339	0.430	0.341	0.251	0.366	0.175	0.459	0.316	0.235	0.192	0.352	0.445	0.297	0.339
Cl	0.030	0.032	0.013	0.005	0.016	0.000	0.022	0.007	0.012	0.008	0.032	0.071	0.013	0.008	0.009	0.041	0.045	0.015
Mg Tot	4.122	4.156	3.759	3.894	4.805	4.344	4.710	4.827	4.940	5.041	4.328	4.130	4.675	4.714	3.913	3.138	3.699	4.303
Total cations	14.477	14.504	14.451	14.644	14.316	14.421	14.286	14.219	14.320	14.175	14.459	14.316	14.235	14.192	14.295	14.445	14.261	14.316

Note: EMP = electron microprobe; Anl # = analysis identification number.

Table 1 (continued).

Hole, core, section	1028A-15X-6	1028A-15X-6	1028A-15X-6	1028A-15X-7	1028A-15X-7	1028A-15X-7	1028A-15X-7	1028A-15X-7	1028A-15X-7	1032A-13R-2	1032A-13R-3	1032A-13R-3	1032A-13R-3	1032A-13R-3	1032A-13R-3	1032A-13R-3
Piece	2	2	2	2	2	2	2	2	2	17	5	5	5	5	5	5
Interval (cm)	130-132	130-132	130-132	15-18	15-18	15-18	15-18	15-18	15-18	136-143	38-42	38-42	38-42	38-42	38-42	38-42
Occurrence	Vesicle	Vesicle	Vesicle	Vesicle	Vesicle	Vesicle	Vesicle	Vesicle	Vesicle	Vein	Vesicle	Vesicle	Vesicle	Vesicle	Vesicle	Vesicle
EMP Anl #	112	114	115	116	117	118	119	120	121	125	129	130	131	132	133	134
SiO_2	50.00	51.96	54.10	48.75	46.90	52.39	50.07	49.75	47.90	48.17	48.82	47.30	47.82	48.53	50.11	48.33
TiO_2	0	0.05	0	0.08	0.07	0	0.01	0.11	0.02	0	0.04	0.04	0.07	0	0.10	0.05
Al_2O_3	2.89	3.13	1.93	3.87	5.07	2.59	3.13	3.93	4.47	3.78	3.45	4.03	3.97	4.38	3.62	4.40
FeO	10.59	11.22	12.31	8.93	11.55	8.52	9.17	10.16	11.64	11.60	8.14	10.74	9.61	12.30	8.78	11.22
MnO	0	0.14	0.09	0	0	0.04	0.16	0.12	0.14	0.03	0	0	0.11	0.13	0.12	0.02
MgO	19.76	21.15	21.28	20.23	18.8	22.30	20.91	20.95	19.92	18.98	21.18	19.47	20.17	19.20	21.72	19.96
CaO	0.47	0.55	0.44	0.55	0.81	0.38	0.40	0.60	0.68	0.58	0.60	0.65	0.80	0.46	0.62	0.60
Na_2O	0.64	0.68	0.50	0.78	0.60	0.65	0.70	0.93	0.95	1.01	0.93	0.84	0.90	1.12	0.83	0.86
K_2O	0.27	0.19	0.27	0.13	0.04	0.26	0.23	0.12	0.04	0.44	0.22	0.22	0.12	0.25	0.32	0.45
Cl	0.05	0.06	0.05	0.13	0.02	0.08	0.10	0.07	0.04	0.06	0.04	0.05	0.04	0.09	0.08	0.07
Ba																
Total	84.67	89.13	90.97	83.45	83.86	87.21	84.88	86.74	85.8	84.65	83.42	83.34	83.61	86.46	86.3	85.96
O = Cl	0.01	0.01	0.01	0.03	0.00	0.02	0.02	0.02	0.01	0.01	0.01	0.01	0.01	0.02	0.02	0.02
Total	84.66	89.12	90.96	83.42	83.86	87.19	84.86	86.72	85.79	84.64	83.41	83.33	83.60	86.44	86.28	85.94
# of oxygen	22	22	22	22	22	22	22	22	22	22	22	22	22	22	22	22
Tetrahedral Cations																
Si(IV)	7.601	7.524	7.687	7.473	7.265	7.635	7.549	7.392	7.270	7.415	7.466	7.357	7.369	7.335	7.436	7.311
Al(IV)	0.399	0.476	0.313	0.527	0.735	0.365	0.451	0.608	0.730	0.585	0.534	0.643	0.631	0.665	0.564	0.689
Sum of (IV)	8.000	8.000	8.000	8.000	8.000	8.000	8.000	8.000	8.000	8.000	8.000	8.000	8.000	8.000	8.000	8.000
Octahedral																
Al(VI)	0.120	0.059	0.011	0.173	0.191	0.080	0.106	0.081	0.070	0.101	0.088	0.097	0.091	0.116	0.069	0.096
Fe^{2+}	1.346	1.359	1.463	1.145	1.496	1.038	1.156	1.263	1.478	1.493	1.041	1.397	1.239	1.555	1.090	1.420
Mn	0.000	0.017	0.011	0.000	0.000	0.005	0.020	0.015	0.018	0.004	0.000	0.000	0.014	0.017	0.015	0.003
Ti	0.000	0.005	0.000	0.009	0.008	0.000	0.001	0.012	0.002	0.000	0.005	0.005	0.008	0.000	0.011	0.006
Mg	4.477	4.560	4.506	4.622	4.304	4.843	4.699	4.629	4.432	4.354	4.827	4.501	4.632	4.313	4.803	4.476
Sum of (VI)	5.943	6.000	5.991	5.949	6.000	5.967	5.983	6.000	6.000	5.953	5.961	6.000	5.984	6.000	5.989	6.000
Interlayer																
Mg	0.000	0.005	0.000	0.000	0.036	0.000	0.000	0.011	0.074	0.000	0.000	0.012	0.000	0.012	0.000	0.024
Ca	0.077	0.085	0.067	0.090	0.134	0.059	0.065	0.096	0.111	0.096	0.098	0.108	0.132	0.074	0.099	0.097
Na	0.189	0.191	0.138	0.232	0.180	0.184	0.205	0.268	0.280	0.301	0.276	0.253	0.269	0.328	0.239	0.252
K	0.052	0.035	0.049	0.025	0.008	0.048	0.044	0.023	0.008	0.086	0.043	0.044	0.024	0.048	0.061	0.087
Sum interlayer	0.318	0.316	0.254	0.348	0.358	0.291	0.314	0.397	0.472	0.484	0.417	0.417	0.425	0.463	0.398	0.461
Cl	0.013	0.015	0.012	0.034	0.005	0.020	0.026	0.018	0.010	0.016	0.010	0.013	0.010	0.023	0.020	0.018
Mg Tot	4.477	4.564	4.506	4.622	4.340	4.843	4.699	4.639	4.506	4.354	4.827	4.513	4.632	4.325	4.803	4.500
Total cations	14.261	14.316	14.245	14.297	14.358	14.259	14.296	14.397	14.472	14.436	14.378	14.417	14.409	14.463	14.386	14.461

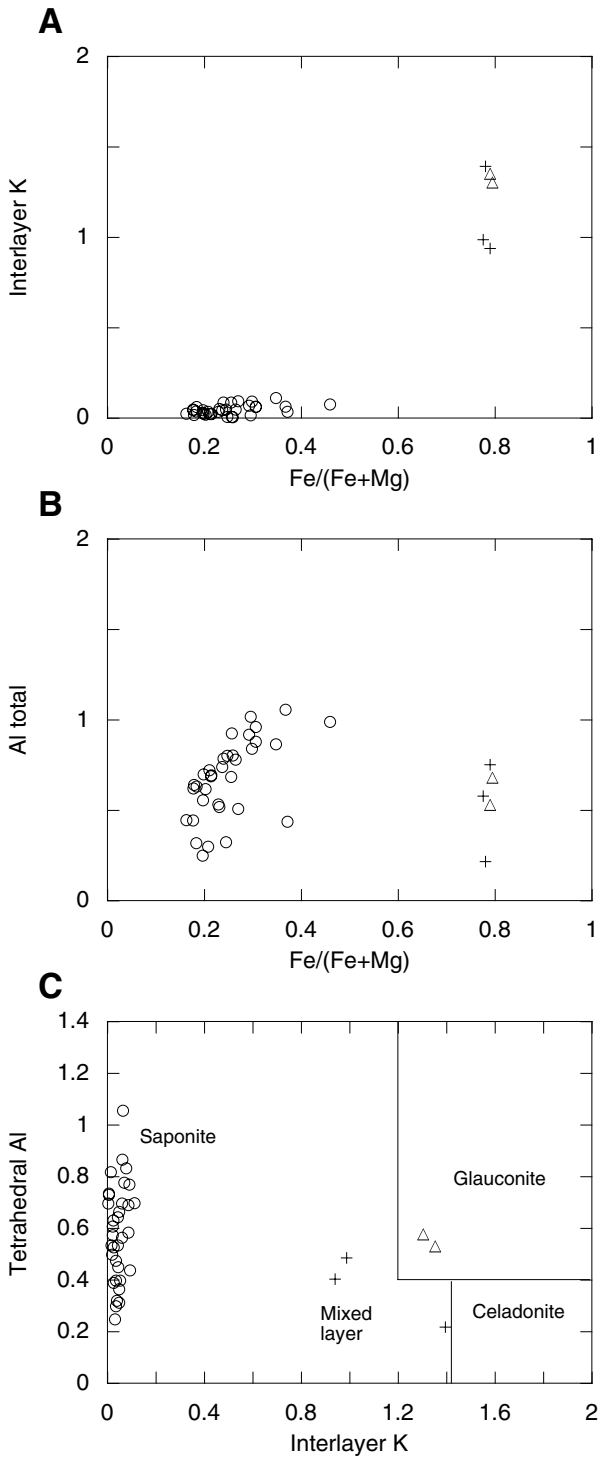

Figure 3. Results of electron microprobe analyses of clay minerals. Units are moles per $O_{20}(OH)_4$ from the calculated structural formulas in Tables 1 and 2. Note that ideal celadonite will contain two interlayer cations. **A.** Interlayer K plotted against Fe/(Fe + Mg). Saponites (open circles) group near K = 0, and celadonitic clays (crosses, triangles) exhibit K < 2. **B.** Al total plotted against Fe/(Fe + Mg). **C.** Tetrahedral Al plotted against Interlayer K^+. Mineral names are from Teagle et al. (1996). Saponites are open circles; celadonitic clays include the triangles, which plot as glauconite, and the crosses, which plot as "mixed-layer" clays.

average Mg# (Mg# = Mg/[Mg + Fe^{2+}]) of about 60, whereas the massive ferrobasalts of Hole 1025C have an average Mg# of 45 (Davis, Fisher, Firth, et al., 1997). Saponite from the pillow basalts is, on average, more Mg-enriched than that from the ferrobasalt (Fig. 5). Furthermore, saponite from Leg 148, Hole 896A, from a ridge-flank location near the Costa Rica Rift, is hosted by pillow and massive basalts with a high Mg# (average Mg# = 65.2), and the compositions of those saponites show enrichment in Mg relative to the Leg 168 saponite (Fig. 5). Consequently, the host rock Mg# probably exerts a control on the Mg:Fe value of infiltrating fluid and, thus, on the composition of secondary clay.

The trace element concentrations in saponite (Tables 3, 4) are comparable to those reported by Berndt and Seyfried (1986), who analyzed vein materials from Deep Sea Drilling Project Site 597 basalts that were altered at low temperature. In particular, the Site 597 smectite veins exhibited variable enrichments of transition metals Cr through Zn relative to the host basalts, with a particularly large enrichment of Ni. Analyses of the Leg 168 saponite vein from Hole 1026B (Table 4) gave values for Co (20–70 ppm), Ni (1500–2600 ppm), Cu (50–330 ppm) and Zn (500–1400 ppm) that are similar to or higher than the concentrations in Berndt and Seyfried's (1986) smectite veins: Co (16–88 ppm), Ni (159–287 ppm), Cu (22–531 ppm) and Zn (31–71 ppm). Berndt and Seyfried (1986) attributed enriched Ni concentrations to the fact that Ni^{2+}, which likely is derived from alteration of olivine, may substitute for Mg^{2+} in smectite. This explanation is reasonable for explaining the very high Ni concentrations in the Leg 168 saponites as well, particularly because some olivine phenocrysts from this site were observed to contain millerite(?) inclusions (Davis, Fisher, Firth, et al., 1997), indicating a high Ni concentration. The very high enrichment of Zn in Leg 168 saponite may reflect a local source that is particularly rich in Zn, either a primary magmatic material or a hydrothermal deposit.

Numerous previous studies of trace elements during low-temperature alteration have focused on bulk whole-rock analyses of complementary fresh and altered material. For example, Ludden and Thompson (1979) note that palagonitized seafloor basalts exhibit enrichments in light rare earth elements (LREE), whereas the heavy rare earth elements (HREE) are essentially unchanged during low-temperature seafloor weathering. Daux et al. (1994) report the same behavior for basalts subjected to freshwater weathering, and further note that Th is enriched along with the LREE. Jochum and Verma (1996) note enrichments in LREE, Zr, Hf, Nb, and Sr, whereas the HREE and Y are not affected by seawater alteration of MORBs. Additionally, Hart and Staudigel (1982) indicate that Rb and U are enriched in MORBs altered at low temperature as well.

The trace element data available for Leg 168 saponite samples show that this clay, relative to the original basalt, is enriched in Rb, Th, and U; however, LREE are not enriched relative to HREE, and HREE, Y, Zr, Hf, Nb, and Sr are generally depleted (Fig. 4). This suggests that Rb, Th, and U enrichment in altered seafloor basalts may be explained by the presence of secondary smectite, but the enrichment of LREE, Y, Zr, Hf, Nb, and Sr cannot. Other candidate host phases for these elements could be the secondary $Fe(O,OH)_x$, which is nearly ubiquitous in alteration haloes formed under oxidizing conditions, and palagonite. Finally, because the Leg 168 saponite exhibits about the same degree of depletion of both LREE and HREE, its formation does not apparently lead to fractionation of the REE.

ACKNOWLEDGMENTS

We wish to thank the Master and crew of *JOIDES Resolution* for Leg 168, the Ocean Drilling Program personnel, and the other members of the shipboard scientific party, all of whom worked together to

Table 2. Representative electron microprobe celadonite analyses.

Hole, core, section:	1027C-4R-1	1027C-4R-1	1027C-4R-1	1027C-4R-1	1026B-2R-1	1026B-2R-1
Piece:	18	18	18	15	1	1
Interval (cm):	114-118	114-118	114-118	93-96	0-3	0-3
Occurrence:	Vesicle	Vesicle	Vesicle	Replacement	Vesicle	Vesicle
EMP Anl #:	2	3	4	25	100	101
SiO_2	47.06	47.90	50.33	52.21	50.58	50.65
TiO_2	0.05	0.01	0.00	0.00	0.07	0.07
Al_2O_3	3.67	2.90	1.20	2.09	3.31	4.26
FeO(tot)	23.34	24.65	24.75	18.45	24.36	22.95
FeO(calc)	1.19	0.22	1.81	0.00	0.00	1.23
Fe_2O_3(calc)	24.58	27.12	25.47	20.48	27.04	24.11
MnO	0.13	0.03	0.00	0.05	0.02	0.00
MgO	3.39	3.67	3.91	7.41	3.95	3.43
CaO	0.57	0.54	0.41	0.29	0.67	0.76
Na_2O	0.17	0.23	0.29	0.14	0.45	0.48
K_2O	6.48	6.84	7.13	8.00	5.21	4.91
Cl	0.02	0.05	0.06	0.02	0.02	0.03
Ba	0.00	0.00	0.03	0.00		
Total	87.32	89.51	90.63	90.69	91.32	89.93
O = Cl	0.00	0.01	0.01	0.00	0.00	0.01
Total	87.31	89.50	90.62	90.68	91.32	89.92
# IV + VI cations	12.00	12.00	12.00	12.00	12.00	12.00
Tetrahedral Cations						
Si(IV)	7.422	7.425	7.719	7.768	7.513	7.597
Al(IV)	0.578	0.530	0.217	0.232	0.487	0.403
Sum(IV)	8.000	7.955	7.936	8.000	8.000	8.000
Octahedral						
Al(VI)	0.105	0.000	0.000	0.135	0.093	0.350
Ti	0.006	0.001	0.000	0.000	0.008	0.008
Fe^{2+}	0.157	0.028	0.232	0.000	0.000	0.154
Fe^{3+}	2.918	3.164	2.939	2.294	3.023	2.722
Mn	0.017	0.004	0.000	0.006	0.003	0.000
Mg	0.797	0.848	0.894	1.643	0.874	0.767
Sum(VI)	4.000	4.045	4.064	4.078	4.000	4.000
Interlayer						
Ca	0.096	0.090	0.067	0.046	0.107	0.122
Na	0.052	0.069	0.086	0.040	0.130	0.140
K	1.304	1.353	1.395	1.519	0.987	0.940
Cl	0.005	0.013	0.016	0.005	0.005	0.008
Total	13.452	13.525	13.564	13.688	13.229	13.201
Al(VI)/[Al(VI) + Fe^{3+}]	0.035	0.000	0.000	0.055	0.030	0.114
Mg/(Mg + Fe^{2+})	0.835	0.968	0.794	1.000	1.000	0.833

Note: EMP = electron microprobe; Anl # = analysis identification number.

Table 3. Conventional nebulization ICP-MS analyses of bulk clays.

Hole, core, section:	1026B-3R-1	1026B-3R-1	1026B-4R-1	1025C-2R-1	1032A-13R-4
Piece:	12	4	2	16	4
Interval (cm):	74-78	29-34	7-11	134-137	21-29
Occurrence:	Vein	Breccia	Vein	Vesicle	Vein
Ba	55.89	126.12	24.35	27.60	10.08
Rb	8.91	5.45	0.00	0.44	9.04
Th	0.00	0.48	0.00	0.00	0.00
U	1.46	0.50	0.00	0.00	0.00
Nb	2.71	3.03	0.00	0.00	0.86
Ta	0.00	0.00	0.00	0.00	0.00
La	1.07	1.80	2.43	0.94	0.18
Ce	2.52	3.20	11.89	3.10	2.14
Sr	39.74	15.32	77.49	33.53	28.73
Nd	3.98	3.98	10.18	5.04	2.50
Sm	0.00	1.36	5.23	0.00	0.00
Zr	61.89	158.46	32.26	13.79	8.24
Hf	0.21	12.87	0.00	0.16	0.00
Tb	0.03	0.48	0.65	0.30	0.03
Y	6.77	15.59	15.80	12.23	4.41
Tm	0.05	0.35	0.21	0.01	0.01
Yb	0.50	0.86	1.17	1.25	0.19
Lu	0.07	0.31	0.18	0.41	0.05

Note: All values are in ppm.

make Leg 168 a success. Chris Fleisher assisted in electron microprobe analysis at the University of Georgia, Crawford Elliott helped with X-ray diffraction analyses at Georgia State, and Michelle Shearer assisted in sample preparation. This study was supported through a JOI/USSAC grant as well as ICP-MS support from the National Science Foundation (EAR-9405716 and EAR-950623). We thank D.R. Peacor, R. Mühe, and C. Escutia for helpful reviews of the original manuscript.

REFERENCES

Adamson, A.C., and Richards, H.G., 1990. Low-temperature alteration of very young basalts from ODP Hole 648B: Serocki volcano, Mid-Atlantic Ridge. *In* Detrick, R., Honnorez, J., Bryan, W.B., Juteau, T., et al., *Proc. ODP, Sci. Results,* 106/109: College Station, TX (Ocean Drilling Program), 181–194.

Alt, J.C., 1993. Low-temperature alteration of basalts from the Hawaiian Arch, Leg 136. *In* Wilkens, R.H., Firth, J.V., Bender, J., et al., *Proc. ODP, Sci. Results,* 136: College Station, TX (Ocean Drilling Program), 133–146.

Alt, J.C., Honnorez, J., Laverne, C., and Emmermann, R., 1986. Hydrothermal alteration of a 1 km section through the upper oceanic crust, Deep Sea Drilling Project Hole 504B: mineralogy, chemistry, and evolution of seawater-basalt interactions. *J. Geophys. Res.,* 91:10309–10335.

Anderson, R.N., Langseth, M.G., and Sclater, J.G., 1977. The mechanisms of heat transfer through the floor of the Indian Ocean. *J. Geophys. Res.,* 82:3391–3409.

Berndt, M.E., and Seyfried, W.E., Jr., 1986. B, Li, and associated trace element chemistry of alteration minerals, Holes 597B and 597C. *In* Leinen, M., Rea, D.K., et al., *Init. Repts. DSDP,* 92: Washington (U.S. Govt. Printing Office.), 491–498.

Daux, V., Crovisier, J.L., Hemond, C., and Petit, J.C., 1994. Geochemical evolution of basaltic rocks subjected to weathering: fate of the major elements, rare earth elements, and thorium, *Geochim. Cosmochim. Acta,* 58:4941–4954.

Davis, E.E., Chapman, D.S., Mottl, M.J., Bentkowski, W.J., Dadey, K., Forster, C., Harris, R., Nagihara, S., Rohr, K., Wheat, G., and Whiticar, M., 1992. FlankFlux: an experiment to study the nature of hydrothermal circulation in young oceanic crust. *Can. J. Earth Sci.,* 29:925–952.

Davis, E.E., Fisher, A.T., Firth, J.V., et al., 1997. *Proc. ODP, Init. Repts.,* 168: College Station, TX (Ocean Drilling Program).

Desprairies, A., Tremblay, P., and Laloy, C., 1989. Secondary mineral assemblages in a volcanic sequence drilled during ODP Leg 104 in the Norwegian Sea. *In* Eldholm, O., Thiede, J., Taylor, E., et al., *Proc. ODP, Sci. Results,* 104: College Station, TX (Ocean Drilling Program), 397–409.

Gillis, K.M., Ludden, J.N., Plank, T., and Hoy, L.D., 1992. Low-temperature alteration and subsequent reheating of shallow oceanic crust at Hole 765D, Argo Abyssal Plain. *In* Gradstein, F.M., Ludden, J.N., et al., *Proc. ODP, Sci. Results,* 123: College Station, TX (Ocean Drilling Program), 191–199.

Hart, S.R., and Staudigel, H., 1982. The control of alkalies and uranium in sea water by ocean crust alteration. *Earth Planet. Sci. Lett.,* 58:202–212.

————, 1986. Ocean crust vein mineral deposition: Rb/Sr ages, U-Th-Pb geochemistry, and duration of circulation at DSDP Sites 261, 462 and 516. *Geochim. Cosmochim. Acta,* 50:2751–2761.

Jenner, G.A., Foley, S.F., Jackson, S.E., Green, T.H., Fryer, B.J., and Longerich, H.P., 1993. Determination of partition coefficients for trace elements in high pressure-temperature experimental run products by laser ablation microprobe-inductively coupled plasma-mass spectrometry (LAM-ICP-MS). *Geochim. Cosmochim. Acta,* 57:5099–5103.

Jochum, K.P., and Verma, S.P., 1996. Extreme enrichment of Sb, Tl and other trace elements in altered MORB. *Chem. Geol.,* 130:289–299.

Kontak, D.J., and Jackson, S., 1995. Laser-ablation ICP-MS micro-analysis of calcite cement from a Mississippi-valley-type Zn-Pb deposit, Nova Scotia: dramatic variability in REE content on macro- and micro-scales. *Can. Mineral.,* 33:445–467.

Laverne, C., Belarouchi, A., and Honnorez, J., 1996. Alteration mineralogy and chemistry of the upper oceanic crust from Hole 896A, Costa Rica Rift. *In* Alt, J.C., Kinoshita, H., Stokking, L.B., and Michael, P.J. (Eds.), *Proc. ODP, Sci. Results,* 148: College Station, TX (Ocean Drilling Program), 151–170.

Li, G., Peacor, D.R., Coombs, D.S., and Kawachi Y., 1997. Solid solution in the celadonite family: the new minerals ferroceladonite, $K_2Fe_2^{2+}Fe_2^{3+}Si_8O_{20}(OH)_4$, and ferroaluminoceladonite, $K_2Fe_2^{2+}Al_2Si_8O_{20}(OH)_4$. *Am. Mineral.,* 82:503–511.

Ludden, J.N., and Thompson, G., 1979. An evaluation of the behavior of the rare earth elements during the weathering of sea floor basalt. *Earth Planet. Sci. Lett.,* 43:85–92.

Mottl, M.J., and Wheat, C.G., 1994. Hydrothermal circulation through mid-ocean ridge flanks: fluxes of heat and magnesium. *Geochim. Cosmochim. Acta,* 58:2225–2238.

Perkins, W.T., and Pearce, N.J.G., 1995. Mineral microanalysis by laserprobe inductively coupled plasma mass spectrometry. *In* Potts, P.J., Bowles, J.F.W., Reed, S.J.B., and Cave, M.R. (Eds.), *Microprobe Techniques in the Earth Sciences:* London (Chapman and Hall), 291–325.

Purdy, G.M., 1987. New observations of the shallow seismic structure of young oceanic crust. *J. Geophys. Res.,* 92:9351–9362.

Sclater, J.G., Crowe, J., and Anderson, R.N., 1976. On the reliability of ocean heat flow averages. *J. Geophys. Res.,* 81:2997–3006.

Stein, C.A., and Stein, S., 1994. Constraints on hydrothermal heat flux through the oceanic lithosphere from global heat flow. *J. Geophys. Res.,* 99:3081–3095.

Teagle, D.A.H., Alt, J.C., Bach, W., Halliday, A.N., and Erzinger, J., 1996. Alteration of upper ocean crust in a ridge-flank hydrothermal upflow zone: mineral, chemical, and isotopic constraints from Hole 896A. *In* Alt, J.C., Kinoshita, H., Stokking, L.B., and Michael, P.J. (Eds.), *Proc. ODP, Sci. Results,* 148: College Station, TX (Ocean Drilling Program), 119–150.

Date of initial receipt: 11 December 1998
Date of acceptance: 10 August 1999
Ms 168SR-004

Table 4. Results of LA–ICP-MS analyses of saponite vein from Sample 168-1026B-4R-1, 7–11 cm (Piece 2).

	Co	Ni	Cu	Zn	Rb	Sr	La	Ce	^{206}Pb	^{208}Pb	U
Ablation 1	28	1551	55	668	5	121	BDL	BDL	285	221	BDL
Ablation 2	21	1478	264	521	BDL	118	BDL	13	BDL	BDL	BDL
Ablation 3	49	2596	331	1381	21	303	BDL	64	135	184	BDL
Ablation 4	55	1930	154	646	17	284	BDL	BDL	145	108	BDL
Ablation 5	72	1646	98	553	BDL	93	BDL	BDL	BDL	BDL	BDL
Ablation 6	35	2079	92	669	21	155	BDL	BDL	248	120	BDL
SDL (ppm)	2	28	7	90	2	3	8	5	18	11	6
MDL (ppm)	4	88	16	105	2	48	16	13	13	8	8
RSD (element/Mg)rm (%)	48	34	30	46	58	30	54	32	21	77	63

Notes: All values are in ppm. BDL = below detection limit. SDL = statistical detection limit in ppm for each element determined from counting statistics on the SRM-611 glass standard, which contains about 500 ppm of each element. The SDL is three times the concentration equivalent of the square root of background counts. MDL = minimum detection limit in ppm determined using the equation in Jenner et al. (1993), which takes into account the counting statistics on both standard and specimen. RSD = relative standard deviation of repeat determinations of blank-corrected element counts divided by blank-corrected magnesium counts, expressed as percentage. This value gives a qualitative idea of the errors associated with each analysis.

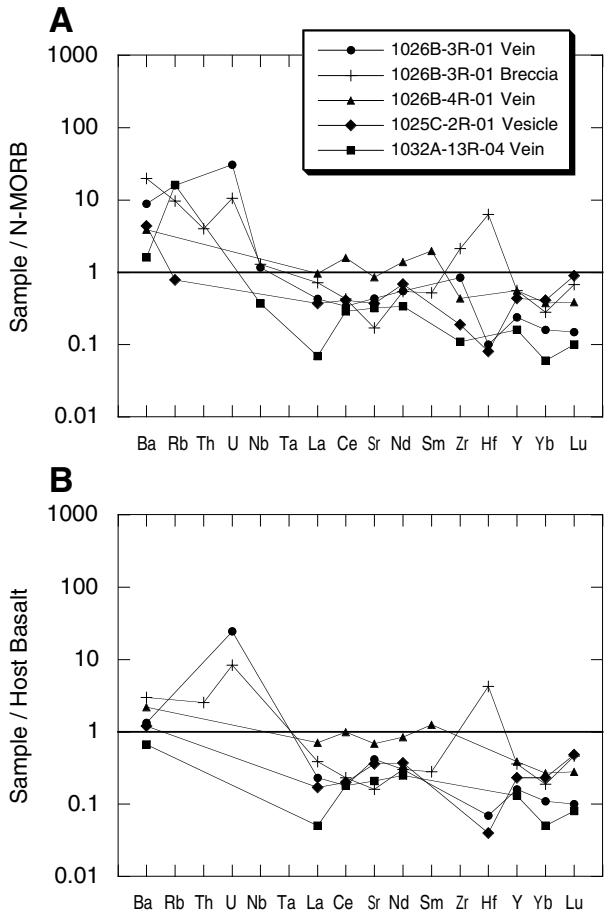

Figure 4. Spider diagrams showing trace element data for five saponite samples, determined by ICP-MS. **A.** Trace elements normalized to average N-MORB. **B.** Trace elements normalized to the trace element concentrations reported for the immediate host rock (M. Constantin, pers. comm., 1998).

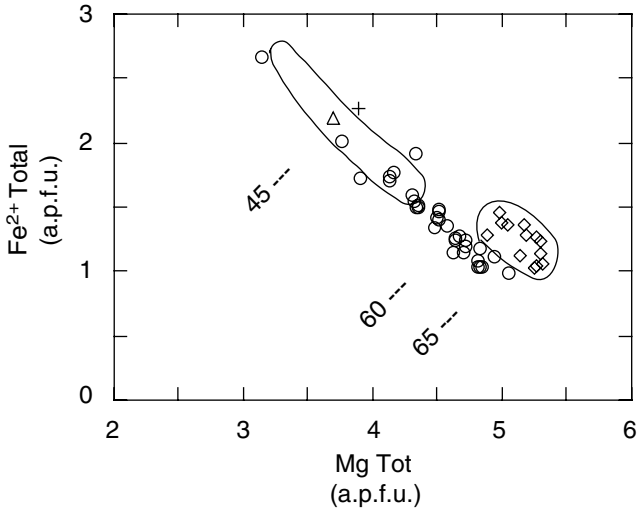

Figure 5. Plot of Fe^{2+} Total vs. Mg Total (atoms per formula unit [a.p.f.u.]) for saponites. Circles = saponites from Leg 168 pillow basalts, which have an average Mg# = [Mg/(Mg + Fe^{2+})] of 60. Diamonds = saponites from Hole 896A pillow basalts and massive basalts, which have an average Mg# of 65 (data of Teagle et al., 1996). Cross = saponite from a diabase from Hole 1027C. Triangle = saponite from a massive ferrobasalt from Hole 1025C. These ferrobasalts have an average Mg# of 45, and the enclosed area labeled "45" shows the range of all saponite compositions from the Hole 1025C ferrobasalts (Marescotti et al., Chap. 10, this volume).